HHS Public Access

Author manuscript

Nat Biomed Eng. Author manuscript; available in PMC 2018 May 27.

Published in final edited form as:

Nat Biomed Eng. 2017 ; 1: 983–992. doi:10.1038/s41551-017-0157-y.

Local and sustained miRNA delivery from an injectable hydrogel promotes cardiomyocyte proliferation and functional regeneration after ischemic injury

Leo L. Wang[1,†], **Ying Liu**[2,†], **Jennifer J. Chung**[3], **Tao Wang**[2], **Ann C. Gaffey**[3], **Minmin Lu**[2], **Christina A. Cavanaugh**[2], **Su Zhou**[2], **Rahul Kanade**[3], **Pavan Atluri**[3], **Edward E. Morrisey**[2,*], and **Jason A. Burdick**[1,*]

[1]Department of Bioengineering, University of Pennsylvania, Philadelphia, PA, 19104

[2]Department of Medicine, University of Pennsylvania, Philadelphia, PA, 19104

[3]Division of Cardiovascular Surgery, Department of Surgery, University of Pennsylvania, Philadelphia, PA, 19104

Abstract

MicroRNA-based therapies that target cardiomyocyte proliferation have great potential for the treatment of myocardial infarction (MI). In previous work, we showed that the miR-302/367 cluster regulates cardiomyocyte proliferation in the prenatal and postnatal heart. Here, we describe the development and application of an injectable hyaluronic acid (HA) hydrogel for the local and sustained delivery of miR-302 mimics to the heart. We show that the miR-302 mimics released in vitro promoted cardiomyocyte proliferation over one week, and that a single injection of the hydrogel in the mouse heart led to local and sustained cardiomyocyte proliferation for two weeks. After MI, gel/miR-302 injection caused local clonal proliferation and increased cardiomyocyte numbers in the border zone of a Confetti mouse model. Gel/miR-302 further decreased cardiac end-diastolic (39%) and end-systolic (50%) volumes, and improved ejection fraction (32%) and fractional shortening (64%) four weeks after MI and injection, compared to controls. Our findings suggest that biomaterial-based miRNA delivery systems can lead to improved outcomes in cardiac regeneration.

[*]**Corresponding Authors:** Edward E. Morrisey, Ph.D., Professor of Medicine and Cell and Developmental Biology, Department of Medicine, University of Pennsylvania, Smilow Translational Research Center, Room 11-124, 3400 Civic Center Boulevard, Bldg 421, Philadelphia, PA 19104, emorrise@mail.med.upenn.edu, Jason A. Burdick, Ph.D., Professor of Bioengineering, Department of Bioengineering, University of Pennsylvania, 240 Skirkanich Hall, 210 S. 33rd Street, Philadelphia, PA 19104, burdick2@seas.upenn.edu, Correspondence and request for materials should be addressed to E.E.M. or J.A.B.

[†]Authors contributed equally

Author Contributions:

L.L.W. and Y.L. contributed equally to this work. L.L.W., Y.L., E.E.M., and J.A.B. conceived the ideas and designed the experiments. L.L.W., Y.L., J.J.C., T.W., A.C.G., M.L., C.A.C., S.Z., and R.K. conducted the experiments and analyzed the data. L.L.W., Y.L., P.A., E.E.M., and J.A.B. interpreted the data and wrote the manuscript. All authors have given approval to the final version of the manuscript.

Competing interests statement:

Provisional patents concerning the technology described in this work have been filed.

Heart disease is the leading cause of mortality across the world - in the United States and Europe, heart disease contributes to 600,000 and 4,000,000 deaths each year, respectively.[1,2] Myocardial infarctions (MI), or heart attacks, are individually linked to at least 50% of deaths.[2] During MI, blood supply to cardiac tissue is compromised, initiating a tissue remodeling response. Central to this process is the permanent loss of contractile cardiomyocytes, the native muscle cell in the heart, and the replacement of healthy tissue with non-contractile, fibrotic tissue. Improved management of acute MI through medical and surgical intervention has allowed up to 95% of patients to survive hospitalization[2]; however, many of these patients will develop chronic heart failure, resulting in a 50% mortality rate at five years post-MI.[2]

Since a hallmark of MI is cardiomyocyte cell death, increasing the number of cardiomyocytes within the damaged myocardium may improve cardiac function. The major challenge to this approach is the limited capacity for renewal of cardiomyocytes in the adult heart.[3,4] Cardiomyocytes are often thought of as being terminally differentiated, exiting the cell cycle within the first week postnatally with low to non-existent levels of proliferation after injury.[5,6] This limited renewal capacity exacerbates the damage from ischemic injury during MI, as damaged cells are replaced with fibrotic scar tissue rather than contractile cardiomyocytes.[7]

Cellular therapy for cardiac regeneration remains an unmet challenge in the treatment of MI. Many cell types have been used in attempts to replace lost cardiomyocytes, including mesenchymal stem cells,[8,9] skeletal myoblasts,[10] and embryonic[11] or induced pluripotent stem cell derived cardiomyocytes.[12] However, only cardiomyocytes derived from pluripotent stem cells have been shown to engraft and produce functional myocardium. An alternative to cell delivery is to promote endogenous cardiomyocyte proliferation using growth factors, small molecules, and gene transfer.[13–15] Among these strategies, certain microRNAs (miRNAs) induce cardiomyocyte proliferation, sometimes leading to improved cardiac function.[16,17]

miRNAs are 18–22 nucleotide long double-stranded RNAs that regulate gene expression post-transcriptionally by base-paring with the 3’ untranslated region (UTR) of target messenger RNAs (mRNAs) and inhibiting their expression. In our previous work, we identified a cluster of miRNAs (miR-302/367) that induced proliferation in cardiomyocytes through a direct binding site on the 3’ UTR of Mst1, Lats2, and Mob1, leading to inhibition of Hippo signaling. Consequently, Yap, the transcriptional effector of the Hippo pathway, translocated to the nucleus to interact with the TEAD transcription factor family to activate gene expression pathways that promote cellular proliferation.[18] In mice, constitutive expression of the miR-302–367 cluster led to cardiomyopathy after MI due to persistent de-differentiation in cardiomyocytes. However, systemic daily administration of miR-302 mimics for one week after MI promoted cardiac regeneration by transiently reactivating the cardiomyocyte cell cycle to increase cell number, leading to proliferation and improved function. This work served as a proof of concept for miR-302 in regeneration; yet, systemic delivery had significant limitations including potential off-target organ accumulation and the need for serial daily administrations.

Here, we demonstrate the use of local intramyocardial delivery of miR-302 mimics to infarcted myocardium via an injectable hydrogel, in an attempt to achieve miR-302 translation and overcome the limitations of systemic delivery. Hydrogels are water-swollen, cross-linked polymers capable of encapsulating and releasing therapeutics after injection into tissues.[19,20] Hydrogels have been explored widely for injection into cardiac tissue[21–26] and several formulations are currently in clinical trials and have demonstrated safety in humans.[27] Hydrogels can be designed to undergo shear-thinning, in which physical crosslinks are reversible under shear stress, which allows them to be injected through a syringe or catheter.[28] We previously developed shear-thinning, injectable hydrogels based on the guest-host interaction of modified hyaluronic acid (HA), a naturally occurring glycosaminoglycan.[23–25] HA was modified with β-cyclodextrin (CD, host) or adamantane (AD, guest), where CD and AD form complexes in a defined structural arrangement with high affinity ($K_a \sim 1 \times 10^5\ M^{-1}$). Thus, when CD-modified HA is mixed with AD-modified HA, they form a hydrogel that exhibits shear-thinning behavior during injection and rapid re-healing after removal of shear, permitting injection into cardiac tissue.[22,23,25,29]

In this work, we utilize this guest-host HA hydrogel system to form injectable gel/miR-302 complexes that release miR-302 to promote cardiomyocyte proliferation and regeneration after MI. Moreover, the gel/miR-302 induced cardiomyocyte proliferation leads to recovery of cardiac function. Thus, a combined gel/miRNA approach can be effectively used to promote mammalian cardiac regeneration through temporal specific activation of cardiomyocyte proliferation.

Cholesterol-modified mimics and CD–HA interaction

We previously identified miR-302b and miR-302c as active miRNAs in the miR-302–367 cluster that modulates Hippo signaling, leading to cardiomyocyte proliferation.[18] To improve cellular uptake, miR-302b and miR-302c were modified with cholesterol on the 5' end of the passenger strand. As previously reported, cholesterol-modified double-stranded RNAs are passively internalized by cells *in vitro* and *in vivo* while unmodified RNAs are naturally repelled by cells due to electrostatics.[30–33] To ensure that cholesterol modifications improved miR-302 mimic uptake, miR-302b and miR-302c with and without cholesterol modifications were added to mouse neonatal cardiomyocytes in culture and cells were stained with antibodies against Ki67, a marker for proliferation. Cardiomyocytes treated with cholesterol-modified miR-302b and miR-302c mimics (miR-302-chol) were significantly more proliferative ($Ki67^+$) than those treated with unmodified mimics (Supplementary Figure 1a,b). Moreover, treatment of cardiomyocytes with cholesterol-modified mimics also led to intracellular expression of miR-302 and knockdown of its Hippo signaling targets Lats2, Mob1, and Mst1 (Supplementary Figure 1c,d).[18] Future studies were performed with equimolar amounts of miR-302b and miR-302c, hereafter simply termed miR-302.

Cholesterol is hydrophobic and has been well-described as a guest for interaction with CD as a host, suggesting that cholesterol-modified mimics may have improved affinity for CD-HA (Figure 1a).[34,35] To examine this interaction, we developed a fluorometric binding assay adapted from other similar assays.[36,37] Rhodamine B (Rho) fluorescence was quenched by

CD-HA due to guest-host interactions between CD and Rho; however, cholesterol has a higher affinity for CD and should displace Rho and recover fluorescence. We observed that adding cholesterol-modified miR-302 increased the fluorescence of the solution suggesting that cholesterol-modified miR-302 bound to CD–HA in a dose-dependent fashion (Figure 1b, Supplementary Figure 2a,b). In contrast, un-modified miR-302 did not change the solution fluorescence, suggesting minimal interaction (Supplementary Figure 2c). Assuming negligible Rho binding, a binding constant for miR-302-chol/CD–HA complex formation was approximated as $K_a = 2.0 \times 10^3\ M^{-1}$ by fitting to the Benesi-Hildebrand equation, in agreement previous reports (Supplementary Figure 2d,e).[38] Cholesterol-modified miR-302 mimics were then assembled into gels with CD-HA and AD-HA (~20% modification of HA with either CD or AD, Supplementary Figure 3). Release of cholesterol-modified miR-302 was sustained from gels over three weeks (Figure 1c), which was slower than the release of mimics without cholesterol, confirming the cholesterol/CD interaction (Supplementary Figure 4).

To confirm that cholesterol-modified miR-302 did not affect mechanical and erosion behavior of gels, we performed oscillatory rheology and gel erosions assays with and without encapsulated miR-302. Storage (G') and loss (G'') moduli were equivalent for gels with and without encapsulated cholesterol-modified miR-302 (Supplementary Figure 5a). Shear-yielding and recovery were also observed in response to alternating high and low strain, demonstrating the ability of these gels to thin under shear strain and rapidly reassemble upon cessation of strain, permitting injection and rapid recovery of the gel/miR-302 system (Supplementary Figure 5b). Gel erosion was not affected by inclusion of cholesterol-modified miR-302 in the system (Supplementary Figure 6). Taken together, cholesterol-modification of miR-302 mimics serves to both enhance cellular uptake and improve affinity for the gel without compromising gel mechanics, shear-thinning, or erosion.

In vitro bioactivity of gel/miR-302 assemblies

To assess the effect of gel/miR-302 assemblies on cardiomyocyte proliferation *in vitro*, supernatants from gel assemblies with miR-302 were collected and replaced serially over two weeks (Figure 2a). Neonatal mouse cardiomyocytes were treated with supernatants from gel/miR-302 or controls and stained with DAPI and antibodies to detect Ki67 and cardiac Troponin T (cTnT). Gel/miR-302 assemblies significantly enhanced proliferation (~20–25% positive for $Ki67^+cTnT^+$) from D0-D1, D1-D4 and D4-D7 compared to gels with a non-specific sequence (gel/miR-NC) or gels alone (~10% positive for $Ki67^+cTnT^+$) (Figure 2b,c). At early time intervals (D0-D1, D1-D4, and D4-D7), between ~0.15–0.3 μg/μL (5–10 μM) of miR-302 was released (Supplementary Figure 7), which we showed is biologically active (Supplementary Figure 1) and induced neonatal cardiomyocyte proliferation. At later time intervals (D7-D10, D10-D14, D14-D21), ~0.1 μg/μL miR-302 was released, leading to no proliferation compared to controls. Since our previous study showed that transient delivery of miR-302 for one week could enhance cardiac function *in vivo*, the gel release profile *in vitro* suggests that gel/miR-302 may replicate serial dosing for one week from a single gel injection.

In vivo bioactivity of gel/miR-302 after cardiac injection

Neonatal cardiomyocytes retain some proliferative capacity and therefore may be more responsive to miR-302 stimulation; thus, we sought to test the bioactivity of gel/miR-302 assemblies in adult cardiomyocytes, which have extremely limited capacity to proliferate both *in vitro* and *in vivo*. Gels were ejected from 27G × 1/2" tuberculin syringes into water to demonstrate their capacity for injection with rapid reassembly and minimal cargo loss (Figure 3a). Gels were then injected in two regions (2 × 5 μL) inferior and lateral to the proximal left anterior descending artery (LAD) in non-infarcted hearts of adult male mice, corresponding to the border zone of the infarct (Figure 3b). At 5, 14, or 28 days, hearts were stained for markers of cardiac proliferation, Ki67 and phosphorylated histone H3 (pH3), and a marker of cytokinesis, Aurora B kinase (Aurora B). Sites of injection were identified from Troponin T negative areas and proliferation in cardiomyocytes (Troponin T positive) was quantified around these sites of injection for all three markers.

Gel/miR-302 injections significantly increased the proportion of $Ki67^+$ cardiomyocytes (Figure 3c). Cardiomyocyte proliferation was sustained at D5 and D14 in gel/miR-302 compared to gel/miR-NC, but was no longer present by D28 (Figure 3e). Gel/miR-302 also induced non-myocyte proliferation at D14 and D28, although at lower levels than both groups at D5 (Supplementary Figure 8a). $pH3^+$, and Aurora B^+ cardiomyocytes around the site of gel/miR-302 injection were also elevated compared to controls at five days (Figure 3d), demonstrating up to ~3% and ~2% of cardiomyocytes staining positive for these proliferation markers (Figure 3f,g).

Of note, gel/miR-302 led to significantly more cardiomyocyte proliferation than PBS/miR-302 (Supplementary Figure 8b), suggesting sustained release and improved retention of miR-302 by the gel in vivo. Injections with gel/miR-NC also led to very low levels (<1%) of cardiomyocytes staining for of Ki67, pH3 and Aurora B, corroborating the very rare and limited capacity for adult cardiomyocyte self-renewal.[39,40] Proliferating cardiomyocytes and non-myocytes were found within <200 μm of injection (Supplementary Figure 8c). To confirm that cardiomyocytes were proliferating through inhibition of Hippo signaling, sections were stained for Yap. In gel/miR-302 sections, there was increased total Yap in the nucleus in support of our established mechanism by which Yap dephosphorylated and localizes to the nucleus secondary to miR-302 (Supplementary Figure 9).[18] No differences in cardiomyocyte maturity were observed following stimulation (Supplementary Figure 10),

Clonal proliferation in MHC-Confetti mouse model

To verify that the proliferation observed after gel/miR-302 treatment could generate new cardiomyocytes after MI, lineage tracing analysis was performed using a multicolor R26R-Confetti Cre-reporter system with loxP-flanked nuclear green fluorescent protein (nGFP), red fluorescent protein (RFP), yellow fluorescent protein (YFP), and monomeric cyan fluorescent protein (mCFP) (Figure 4a).[41] The construct was designed such that random recombination activates only one of the four fluorescent protein genes, allowing stochastic labeling of target cells and their descendants with a single color. This reporter system also allows cell fate analysis using any inducible Cre activation mouse line (Figure 4b).[41–43]

Confetti mice were bred with the Cre transgene expressed under the myosin heavy chain 6 (Myh6) promoter (Myh6-MerCreMer, also abbreviated MHC-MCM) to express Cre specifically in cardiomyocytes in response to tamoxifen.[44] In this system, Myh6-MerCreMer:R26R-Confetti labeled cells and their daughter cells could express one of four different fluorescent reporters: nGFP, YFP, RFP, or mCFP.

Tamoxifen doses were titrated to ensure low levels of $Myh6^+$ cardiomyocyte labeling so that individual clones could be identified (Supplementary Figure 11a). After tamoxifen, MI was induced by ligation of the LAD. Gel/miR-302 or gel/miR-NC (2 × 5 μL) was then injected adjacent to the infarct in the border zone. At 4 weeks, gel/miR-302 injected hearts were strongly labeled in the infarct border zones (Figure 4c), suggesting increased lineage labeled cardiomyocytes due to clonal expansion. In contrast, gel/miR-NC injected hearts exhibited sparse labeling that mimicked hearts prior to injection (Supplementary Figure 11b). Confocal imaging revealed expression of nGFP, RFP, and YFP in adult hearts injected with both gel/miR-NC and gel/miR-302 (Supplementary Figure 12a). In our hands, the expression of mCFP was too weak to reliably detect, as previously reported.[41,42]

Clonal cardiomyocytes expressing nGFP, RFP, and YFP were clearly identified in gel/miR-302-injected hearts while few clones were observed from gel/miR-NC injection (Supplementary Figure 12a,b). Among labeled cardiomyocytes, multiple clusters expressing nGFP were detected in gel/miR-302 injected hearts and localized to the border zone of the infarction (Supplementary Figure 12a). The average distance between $nGFP^+$ cells was significantly lower in gel/miR-302 treated groups, suggesting that these cells were derived from a common single cell (Supplementary Figure 12c,d). Further analysis with Wheat Germ Agglutinin (WGA) staining to identify cell membranes showed fluorescent cells within 50 μm were mostly contiguous in gel/miR-302 treated groups but not in gel/miR-NC groups (Figure 5a). No differences in cardiomyocyte size were observed in the three fluorescent channels using WGA to distinguish between cardiomyocytes (Supplementary Figure 12e). In gel/miR-NC groups, distant cells (>50 μm) were often interspersed by unlabeled cardiomyocytes. Using 50 μm as a standard, we quantified the number of cells to a single clone for nGFP, RFP, and YFP across all sections of the heart in the border zone of infarcts. Gel/miR-302-injected hearts had a significant increase in the number of cells per clone (as many as 8), suggesting that these cells were derived from a common parent cell that had divided (Figure 5b). Our results demonstrating expansion of clones parallel those of other reports that have used this system.[45–47]

Gel/miR-302 complex pharmacokinetics

To demonstrate that miR-302 mimics were localized and sustained in the heart after MI, the gel was labeled with a near-infrared fluorescent molecule through a Michael addition between a thiolated Cy7.5 dye and methacrylated CD-HA (CD-Me-HA) (Supplementary Figure 13).[23] Cy7.5-labeled CD-HA was then assembled into gels with miR-302 and injected into the heart following MI for *ex vivo* tracking at various times.

Immediately following injection, gels exhibited intense signal surrounding the infarct site at the two injection sites (Figure 6a). This signal declined over the first week and distributed

over the heart, where it dissipated by 28 days. Quantification demonstrated a reduction in radiant efficiency by ~90% over the first week, suggesting highest rates of clearance during this period (Figure 6b). From qPCR, miR-302 expression in the heart was highest at D1, decreased over the first two weeks, and was similar to controls by D28 (Figure 6c). The targets of miR-302, Lats2, Mob1, and Mst1, also decreased in the heart by D7, suggesting bioactivity of the gel/miR-302 complex in modulating these components of Hippo signaling (Figure 6d). Low miR-302 expression was observed in the lungs at D7 (Supplementary Figure 14), suggesting vascular drainage of miR-302 through the coronary sinus.

Cardiac function after MI and gel/miR-302 injection

Recognizing the ability of gel/miR-302 to induce both cardiomyocyte proliferation and clonal, we examined the ability for of gel/miR-302 injections to improve physiological outcomes after MI by echocardiography. Adult mice were selected to receive gel/miR-302, gel/miR-NC, or PBS injection after MI. After four weeks, cardiac function was analyzed through echocardiography and measurements of left ventricular end diastolic volume (LVEDV), left ventricular end systolic volume (LVESV), ejection fraction (EF), and fractional shortening (FS) were made. Gel/miR-302 treated mice had reduced cardiac remodeling, demonstrated by reductions in LVEDV and LVESV, measures of cardiac volumes at the beginning and end of a single contraction, respectively, compared to PBS or gel/miR-NC controls (Figure 7a,b). LVEDV and LVESV of gel/miR-302 treated animals were not significantly different from non-infarcted mice. Whereas PBS and gel/miR-NC treated animals had significantly reduced EF and FS, EF and FS of gel/miR-302 treated animals were not significantly different from non-infarcted mice (Figure 7c,d). Masson's trichrome staining at four weeks shows that the smallest ventricular areas from axial sections were with gel/miR-302 treatment, while gross tissue specimens also demonstrated decreased infarct size (Figure 7e). When quantified, gel/miR-302 appeared to decrease infarct size compared to gel/miR-NC from Masson's trichrome sections, although this effect was not statistically significant (Figure 7f, Supplementary Figure 15). Representative 1-D echocardiographic M-mode measurements of wall movement are shown (Figure 7g), which illustrate improved anterior wall movement and decreased systolic and diastolic inner left ventricular diameters in gel/miR-302 treated mice. No changes in apoptosis or vascular density were observed at D28 between gel/miR-NC and gel/miR-302 treatments to suggest improvements were related to the cardiomyocyte response (Supplementary Figure 16, Supplementary Figure 17).

Discussion

The present study demonstrates that an engineered hydrogel, designed for injection and sustained delivery of miR-302, promotes both cardiomyocyte proliferation and functional regeneration. Our hydrogel system was developed to overcome the limitations of systemic delivery and to replace the requirement for 7 days of serial injections with sustained release from a single gel injection into the myocardium. The guest-host assembly mechanism was particularly attractive for this application as it permitted injection and self-healing to improve retention, and could potentially be adapted to minimally invasive delivery methods

(e.g., catheter). Lastly, the hydrogel was designed from HA, a component used in numerous clinical applications.[48]

To further control release, the guest-host assembly mechanism also presented cyclodextrin that can be used to sequester cholesterol-modified miRNA in the hydrogel. Interestingly, binding of cholesterol to the cyclodextrin had minimal effects on gel erosion and mechanics while sustaining the release of the miRNA mimics over three weeks *in vitro*, slower than when these interactions are not included. Because mimics released faster than the gel eroded, we believe diffusion played a major role in release, likely due to the dynamic interactions within the gel and anionic repulsion between negatively charged HA and RNA. Mimic release may also be sustained due to increase in size by cholesterol modification and the ability for cholesterol to aggregate with itself due to hydrophobicity, causing entrapment within the network.

In vitro, the gel/miR-302 complex led to proliferation in neonatal mouse cardiomyocytes in releasates collected as far out as 7 days. The reduction in proliferation from releasates collected after this time (D10, D15) could be due to RNA degradation given the extended time of the experiment. Remarkably, *in vivo*, our gel/miR-302 complex led to robust proliferation of cardiomyocytes at 5 and 14 days in the adult heart, a terminally differentiated organ. Expression of Aurora B kinase suggested that cardiomyocytes not only entered the cell cycle but were undergoing cytokinesis. Clonal expansion of newly generated cardiomyocytes was observed surrounding the infarct zone of the hearts treated with the gel/miR-302 complex. The use of a multi-colored lineage reporter allowed us to verify the generation of new cardiomyocytes in comparison to simply observing an increase in proliferative markers. Our findings concur with recent data showing that small numbers of newly generated cardiomyocytes observed over the lifespan of mammals or after injury are due to proliferation of pre-existing cardiomyocytes rather than arising from a progenitor population.[39] While these new cells may enhance contractility after MI, cardiomyocytes also play a role in limiting remodeling by signaling through paracrine factors to fibroblasts.[49] This explains the improvements in global cardiac volumes and function observed after delivery of the gel/miR-302 complex. Interestingly, while other gels have improved function after MI, no improvement was observed in our case. This may be related to the softness (~500 Pa) and relative rapid clearance of our gel in the heart. Previous gel formulations that led to cardiac bulking were stiffer with higher retention.[23,25]

The proliferative potential of the gel/miR-302 complex is further attributed to enhanced retention and sustained release of miR-302 mimics upon injection, particularly as there was minimal proliferation without gel. Complexing the miRNA with the gel likely protected the miRNA mimics from degradation by ubiquitous RNAse H mediated mechanisms, allowing for continuous and persistent release of active mimics. This work also builds on previous reports of intramyocardial miRNA injections, where miRNAs were injected naked, in a lipid complex with a transfection reagent.[50,51] Since gels allow for a single application and have been well-tolerated in human trials,[27] we believe the use of a gel/miRNA complex offers significant advantages to these other approaches. Other recent reports have also corroborated the benefit of hydrogels in promoting miRNA delivery to the heart, although with different therapeutic targets or with viral delivery.[52,53]

Our research demonstrates the potential of a bioengineered miRNA delivery approach to promote cardiomyocyte proliferation and cardiac regeneration after MI. This delivery mechanism has distinct advantages over current methods including: (i) overcoming the short lifespan of injected mimics, (ii) use as a single application, (iii) optimization of release of miRNA mimics over times for promoting cardiomyocyte proliferation and cardiac regeneration, and (iv) potential for adaptation to percutaneous delivery through catheter. Currently, there are no approved treatments that regenerate myocardium; in this regard, our system may have unique advantages to other existing treatments for MI. Future studies to refine the gel/miRNA formulation in larger animal models of myocardial infarction are important to progress the gel formulation for *in vivo* delivery. Finally, this study establishes the proof-of-concept of a technology to permit minimally invasive, sustained miRNA delivery that can be tailored towards other small RNAs for application to cardiac and other tissues.

Methods

Material Synthesis

Sodium hyaluronate 74 kDa (LifeCore, Chaska, MN) was converted to a tetrabutylammonium salt (HA-TBA) by exchange against Dowex-100 resin and neutralization by tetrabutylammonium hydroxide. CD-HA and AD-HA were synthesized as previously described.[24] Briefly, CD-HA was prepared by amidation between 6-(6-aminohexyl)amino-6-deoxy-β-cyclodextrin and HA-TBA in the presence of benzotriazol-1-yloxy)tris(dimethylamino)phosphoniumhexafluorophosphate (BOP). AD-HA was synthesized by esterification of HA-TBA with 1-adamantane acetic acid in di-tert-butyl bicarbonate (BOC2O) and 4-dimethylaminopyridine (DMAP). Products were dialyzed, frozen, and lyophilized prior to use. ^{1}H NMR (Bruker) at 360MHz was used to determine final product modification, which was approximately 20% of HA disaccharide repeats for both CD-HA and AD-HA. Me-HA was synthesized by the esterification reaction between HA and methacrylic anhydride and maintenance of pH between 7.5–8.5 for 8 hours. Me-HA was then converted to a TBA salt (Me-HA-TBA) and subsequently modified with CD as previously mentioned. For Cy7.5 labeling, the fluorescent peptide GCKKG-Cy7.5 was synthesized by solid phase peptide synthesis (Protein Technologies) using glycinol 2-chlorotrityl resin and FMOC protected amino acids that was then reacted with the free acid of Cy7.5. To couple the peptide to CD-Me-HA, the peptide was added dropwise to CD-Me-HA in PBS at pH 8 for four hours.

Rheological Characterization

Measurements were performed using an AR2000 stress-controlled rheometer (TA Instruments) fitted with a 20-mm diameter cone and plate geometry, 59 min 42 s cone angle, and 27 μm gap. Rheological properties were examined by time sweeps (1.0 Hz; 0.5% strain). For shear recovery experiments, shear-thinning was performed at 250% strain with recovery at 0.5% strain at 20 Hz.

miRNA purchase

All purchases were made as custom orders from GE Dharmacon. Their sequences are as follows:

cel-miR-67 (miR-NC)

5'-CGCUCAUUCUGCCGGUUGUUAUG-3' (Guide)

3'-AGAUGAGAAAGAUCCUCCAACACU-Chol-5'(Passenger)

mmu-miR-302b (miR-302b)

5'-ACUUUAACAUGGGAAUGCUUUCU-3' (Guide)

3'-GAUGAUUUUGUACCUUCGUGAAU-Chol-5' (Passenger)

mmu-miR-302c (miR-302c)

5'-GCUUUAACAUGGGGUUACCUGC-3' (Guide)

3'-GGUGACUUUGUACCUUCGUGAA-Chol-5' (Passenger)

Unmodified mimics did not have the cholesterol on the 5' of the passenger strand.

Rhodamine Quenching Assay

Rhodamine B (50 ng/μL) was mixed with varying amounts of CD-HA (0–50 ng/μL) towards a final volume of 200 μL in DI H2O to determine saturating CD-HA concentrations for quenching. For unquenching assays, Rhodamine B (50 ng/μL) was quenched with 50 ng/μL CD-HA by mixing. Complexes were then mixed with miR-302 mimics (0–5 μM) in a final volume of 200 μL. Emission was measured on a Tecan Infinite200 96-well microplate reader at an excitation of 550 nm. miR-302b-chol affinity for Rho/CD-HA complexes was calculated by fit to the Benesi-Hildebrand equation.

miR-302 Release and Bioactivity

To form gels with miRNA mimics, CD-HA (3.2 mg) or AD-HA (2.1 mg) polymers were sterilized under UV and resuspended in solutions of miR-302b (210 μM) and miR-302c (210 μM) in PBS under sterile conditions to a final polymer concentration of 5 wt%. Polymer/miRNA solutions of CD-HA and AD-HA were mixed manually and centrifuged. Gels were incubated with OPTI-MEM in 1.5 mL Eppendorf tubes with 500 μL supernatants collected and replaced at D1, D4, D7, D10, D15 and D21. Total miRNA concentration in releasates was quantified by RiboGreen (ThermoFisher) according to manufacturer's protocols. Briefly, 20 μL of releasate was incubated with Hi-Range RiboGreen Buffer in 1x TE buffer to a final volume of 200 μL and fluorescence was measured at excitation of 500 nm and emission of 520 nm on a Tecan Infinite200 96-well microplate reader.

Neonatal Cardiomyocyte Isolation and Culture

Ventricular cardiomyocytes from neonatal mice were isolated as described previously.[17] Briefly, ventricles from neonatal mice (postnatal day 0–3) were separated from atria, cut into pieces, and then subjected to trypsin (0.5%) digestion buffer in calcium free HBSS containing 10mM HEPES and 0.54 mM EDTA under constant stirring. After digestion for

18 hours at 4°C, minced hearts were dissociated with calcium free HBSS supplemented with 10% horse serum, 5% FBS, and 10mM HEPES. Cells were then washed with calcium free DMEM supplemented with 10% horse serum and 5% FBS. After a final wash, the cells were plated on uncoated plastic dishes for 2 hours with media supplemented with 10% horse serum and 5% FBS. Non-attached cells were passed through a cell strainer (70 μm, BD Falcon) and seeded on a gelatin coated 96-well plate at a density of 15,000 cells/well. After incubation for 48 hours, the majority of cells started to beat. Mouse ventricular cardiomyocytes prepared using this procedure consistently yielded a purity of >90%. For proliferation assays, gel/miR-302 releasates or controls were added to cells in 96-well plates for 24 hours. After 48 hours, cells were fixed with 4% paraformaldehyde for 15 min, permeabilized with 0.5% Triton X-100 in phosphate buffered saline (PBS) solution for 10 min, followed by 30 min blocking in 5% donkey serum (Jackson ImmunoResearch). Cells were then stained overnight at 4°C with cardiac Troponin T (ThermoFisher, MS295) and Ki67 (Abcam, ab16667) primary antibodies diluted in blocking solution and then secondary antibodies conjugated to Alex Fluor488 and 555. Images were acquired with a Leica TCS SP8 microscope.

In Vivo Proliferation

Prior to use, polymers were sterilized under UV irradiation for 1 hour. Gels were formed with miRNAs as previously described and manually transferred to a 27-Gx½" U-100 tuberculin syringe (Terumo) under sterile conditions on ice. Male C57BL/6 mice (7–9 weeks) were selected to receive 10 μL total of gel or control injection (2 × 5 μL). Mice were anesthetized with 3% isoflurane in an induction chamber (2L) and endotracheally intubated (Harvard Apparatus Regenerative Technology) with 1% isoflurane. A left lateral thoracotomy was performed at the fourth intercostal space to expose the heart. Injections were made inferolateral to the proximal LAD without infarct. Following injection, the chest was closed in 3 layers with a 3-0 polypropylene suture and animals were allowed to recover. After 5 days, the heart was excised, briefly washed in PBS, weighed, fixed in 4% PFA, embedded in paraffin, and further processed for immunofluorescence. Slides were washed in PBS with 0.05% Tritron X-100 (TBST) and blocked in 10% goat serum followed by incubation with primary antibodies against: cardiac Troponin T (ThermoScientific, MS295), Ki67 (Abcam, ab16667), Histone H3 phosphorylated at serine10 (Cell Signaling, 9701), Aurora B kinase (LSBio, LSB6592), Yap (Cell Signaling, 4912S), von Willebrand Factor (Abcam, ab8822), Troponin I (Abcam, ab10231), ACTC1 (Abcam, ab46805). TUNEL staining (Invitrogen) was performed using the Click-iT Alexa Fluor596 kit according to manufacturer's protocols. After 24 hours, sections were incubated with secondary antibodies conjugated to Alex Fluor488, 555 or 647 (Life Technologies). Nuclei were identified by counter-staining sections with DAPI (Vector Labs). Slides were then mounted in Vectashield. A series of confocal images (z-stack) were acquired either by Leica STED Super-Resolution Microscope or LSM 710 Zeiss. Images were analyzed and constructed by ImageJ software and Imaris (Bitplane). Cells were counted by two blinded independent investigators from a minimum of three representative sections per mouse. All animal procedures were performed in accordance with the Institutional Animal Care and Use Committee at the University of Pennsylvania.

MicroRNA Extraction and Expression of miR-302 and Targets

Male C57BL/6 mice (7–9 weeks) were iinjected with either gel/miR-NC or gel/miR-302 (2 × 5 μL). At set time points after intramyocardial injection, the mice were euthanized and the heart, lung, and liver were collected and rapidly snap-frozen in liquid nitrogen for RNA extraction. RNA isolation was performed as previously described.[54] The Ambion mirVana miRNA Isolation Kit (ThermoFisher) was used to purify samples enriched with small RNA. Reverse transcription was performed with TaqMan MicroRNA Reverse Transcription kit (Applied Biosystems) with 3 μL RNA and RT primer sets (miR-302b: ID:000531) according to manufacturer's instructions. Quantitative real-time PCR was performed using the TaqMan MicroRNA assay kit (Applied Biosystems). Primers used for Mob1, Lats2, and Mst1 were ordered from IDT. These primers were also used for qPCR amplification of these targets in neonatal cardiomyocytes.

Mob1b Primers:

Forward: CTGTGATCCAGCTTCAGGAGGAA

Reverse: TGCCAACTCTCGTCTGTCAA

Lats2 Primers:

Forward: TAAGGGTCCTGCTTCCTGTGTTCT

Reverse: ACCTCTCATGTGAAAGAGGCCCAA

Mst1 Primers:

Forward: CAGGGCCTGCATAACATTTGCTGT

Reverse: TTCCTTGTCTGGCAAAGCCCAAAG

Confetti Mouse Generation

Mice were obtained by breeding *Myh6-MerCreMer* and *R26R-Confetti* reporter mice.

Primers to genotype My6-MerCreMer (MHC-MEM):

Forward: CGTTTTCTGAGCATACCTGGA

Reverse: ATTCTCCCACCGTCAGTACG

Primers to genotype R26R-Confetti:

Forward: AAAGTCGCTCTGAGTTGTTAT

Reverse: CCAGATGACTACCTATCCTC

Intraperitoneal tamoxifen (6.7mg/kg) single injection was used to induce stochastic labeling of cardiomyocytes in Myh6-MerCreMer/R26R-Confetti mice. Doses were titrated to ensure low levels of cardiomyocyte labeling so that individual clones could be identified. Two weeks after tamoxifen injection, hearts were accessed by thoracotomy and the left ventricle was infarcted by ligation of the left anterior descending artery. Mice were selected to receive gel/miR-302 or gel/miR-NC (2 × 5 μL) injections lateral to the infarct in the border zone. 28 days post-surgery and miR302 injection, mice were euthanized to collect tissues. The hearts

were fixed overnight with 2% paraformaldehyde (PFA). After 24 hours, hearts were then transferred to 50% OCT, followed by continuous incubation in 100% OCT. Then hearts in OCT were frozen with dry ice and kept in −80 °C until sectioning. For WGA staining, sections were rehydrated and then incubated for one hour at room temperature with WGA conjugated to Alexa Fluor-647 (Life Technologies, W32466) in PBS. Slides were then rinsed in PBS and mounted in Vectashield.

Myocardial Infarction Model

Male C57BL/6 mice (7–9 weeks) were selected to receive 10 μL total of gel or control injection (2 × 5 μL). Mice were anesthetized with 3% isoflurane in an induction chamber (2L) and endotracheally intubated (Harvard Apparatus Regenerative Technology) with 1% isoflurane. A left lateral thoracotomy was performed at the fourth intercostal space to expose the heart. The LAD was ligated 2 mm below the left auricle and infarction was visualized from blanching of the left ventricle. Injections were made lateral to the infarct. The chest was closed in 3 layers with a 3–0 polypropylene suture and animals were monitored during recovery for signs of stroke or embolization. The number of mice for gel/miR-302 treatment group was at least 11 males to give 80% power to detect an effect size of 1.3 SDs using a two-group *t* test with a 0.05 two-sided significance level. Injections were not blinded (due to variations in consistency between gel and PBS) or randomized.

Near-IR Heart Imaging

At D0, D1, D7, D14, and D28, mice were sacrificed and hearts were explanted and scanned on a LI-COR Pearl® Impulse Small Animal Imaging System (Lincoln, NE) with an excitation filter of 745 nm and emission filter for indocyanine green (ICG). Exposure time was set to 2 seconds and binning factor was set to 4. Intensity was expressed as radiant efficiency and the color scale was set to a minimum of 1×10^7 and maximum of 1×10^8. Total radiant efficiency (photons s^{-1} cm^{-2} steradian^{-1} per μW cm^{-2}) over hearts was normalized by manual measurements over the fluorescent region of interest (ROI), subtracting background measurements, and normalizing to initial radiant efficiency measurements as previously described.[55]

Transthoracic Echocardiography

Mice were anesthetized with 3% isoflurane induction following maintenance at 2% by nose cone. Hair was removed using Nair and limbs were taped onto the metal EKG leads. Echo was performed blinded using a VisualSonic Vevo 2100 system with a 40-MHz transducer for cardiac imaging. The transducer was placed parallel along the long axis of the left ventricle for a long axis view or rotated clockwise for short axis view. Images were analyzed using Vevo200 1.6 VisualSonic software. Left ventricular infernal diameters during systole (LVIDS) and diastole (LVIDD) were obtained from 2D M-mode imaging, where fractional shortening was calculated per the equation EF = [(LVIDD-LVIDS)/LVIDD]. Left ventricular end systolic volume (LVESV) and left ventricular end diastolic volume (LVEDV) were obtained from B-mode imaging by manually tracing the left ventricular endocardial border. Ejection fraction was calculated per the equation EF = [(LVEDV-LVESV)/LVEDV].

Statistical Analysis

All statistics were performed in Graphpad Prism 7. All data are reported as means ± standard deviation (SD) and performed in triplicates unless otherwise indicated. For *in vivo* studies, there was a minimum of three mice per group unless otherwise indicated. Comparisons between two groups were performed by Students t-test with two-tailed criteria and significance determined at $p < 0.05$. For comparison between multiple groups, significance was determined by one-way ANOVA with post hoc testing. Bonferroni correction was used to account for multiple comparisons, with $\alpha = 0.05$. Normality was tested by D'Agostino & Pearson normality test and equal variances by Bartlett's test.

Data Availability

The authors declare that all data supporting the findings of this study are available within the paper and its supplementary information files.

Supplementary Material

Refer to Web version on PubMed Central for supplementary material.

Acknowledgments

The authors thank C. Loebel for assistance with manuscript revisions, C. Chen, C. Venkataraman, A. Trubelja, S. Zaman, J. Gordon, and F. Arisi for assistance with mouse surgeries and histology, J. Galarraga for material contribution, S. Schultz of the Penn Small Animal Imaging Facility for assistance with echocardiography, and the Penn Histology and Gene Expression Core. This work was made possible by financial support from the American Heart Association through an established investigator award (J.A.B.) and predoctoral fellowship (L.L.W.), and the National Institutes of Health (F30 HL134255, UO1 HL100405, U01 HL134745).

References

1. Townsend N, et al. Cardiovascular disease in Europe: epidemiological update 2016. Eur. Heart J. 2016; 37:3232–3245. [PubMed: 27523477]
2. Mozaffarian D, et al. Heart Disease and Stroke Statistics-2015 Update: A Report From the American Heart Association. Circulation. 2014; 131:e29–322. [PubMed: 25520374]
3. Pasumarthi KBS. Cardiomyocyte Cell Cycle Regulation. Circ. Res. 2002; 90:1044–1054. [PubMed: 12039793]
4. Jameel MN, Zhang J. Stem cell therapy for ischemic heart disease. Antioxid. Redox Signal. 2010; 13:1879–97. [PubMed: 20687781]
5. Leone M, Magadum A, Engel FB. Cardiomyocyte proliferation in cardiac development and regeneration: a guide to methodologies and interpretations. Am. J. Physiol. - Hear. Circ. Physiol. 2015; 309:H1237–H1250.
6. Laflamme MA, Murry CE. Heart regeneration. Nature. 2011; 473:326–335. [PubMed: 21593865]
7. Li Y, et al. Acute myocardial infarction induced functional cardiomyocytes to re-enter the cell cycle. Am. J. Transl. Res. 2013; 5:327–35. [PubMed: 23634243]
8. Orlic D, et al. Bone marrow cells regenerate infarcted myocardium. Nature. 2001; 410:701–705. [PubMed: 11287958]
9. Elnakish MT, et al. Mesenchymal Stem Cells for Cardiac Regeneration: Translation to Bedside Reality. Stem Cells Int. 2012; 2012:1–14.
10. Gavira JJ, et al. Autologous skeletal myoblast transplantation in patients with nonacute myocardial infarction: 1-year follow-up. J. Thorac. Cardiovasc. Surg. 2006; 131:799–804. [PubMed: 16580437]

11. Hodgson DM, et al. Stable benefit of embryonic stem cell therapy in myocardial infarction. AJP Hear. Circ. Physiol. 2004; 287:H471–H479.
12. Lalit PA, Hei DJ, Raval AN, Kamp TJ. Induced pluripotent stem cells for post-myocardial infarction repair: Remarkable opportunities and challenges. Circulation Research. 2014; 114:1328–1345. [PubMed: 24723658]
13. Korf-Klingebiel M, et al. Myeloid-derived growth factor (C19orf10) mediates cardiac repair following myocardial infarction. Nat. Med. 2015; 21:140–149. [PubMed: 25581518]
14. Ni TT, et al. Discovering small molecules that promote cardiomyocyte generation by modulating Wnt signaling. Chem. Biol. 2011; 18:1658–68. [PubMed: 22195568]
15. Cheng Y-Y, et al. Reprogramming-derived gene cocktail increases cardiomyocyte proliferation for heart regeneration. EMBO Mol. Med. 2017; 9:251–264. [PubMed: 28011860]
16. Liang D, et al. miRNA-204 drives cardiomyocyte proliferation via targeting Jarid2. Int. J. Cardiol. 2015; 201:38–48. [PubMed: 26298346]
17. Eulalio A, et al. Functional screening identifies miRNAs inducing cardiac regeneration. Nature. 2012; 492:376–81. [PubMed: 23222520]
18. Tian Y, et al. A microRNA-Hippo pathway that promotes cardiomyocyte proliferation and cardiac regeneration in mice. Sci. Transl. Med. 2015; 7:279ra38.
19. Panda NC, et al. Improved conduction and increased cell retention in healed MI using mesenchymal stem cells suspended in alginate hydrogel. J. Interv. Card. Electrophysiol. 2014; 41:117–127. [PubMed: 25234602]
20. Teng CJ, Luo J, Chiu RCJ, Shum-Tim D. Massive mechanical loss of microspheres with direct intramyocardial injection in the beating heart: Implications for cellular cardiomyoplasty. J. Thorac. Cardiovasc. Surg. 2006; 132:628–632. [PubMed: 16935119]
21. Tous E, Purcell B, Ifkovits JL, Burdick JA. Injectable Acellular Hydrogels for Cardiac Repair. J. Cardiovasc. Transl. Res. 2011; 4:528–542. [PubMed: 21710332]
22. Gaffey AC, et al. Injectable shear-thinning hydrogels used to deliver endothelial progenitor cells, enhance cell engraftment, and improve ischemic myocardium. J. Thorac. Cardiovasc. Surg. 2015; 150:1268–1277. [PubMed: 26293548]
23. Rodell CB, et al. Shear-Thinning Supramolecular Hydrogels with Secondary Autonomous Covalent Crosslinking to Modulate Viscoelastic Properties In Vivo. Adv. Funct. Mater. 2014; 25:636–644. [PubMed: 26526097]
24. Rodell CB, Kaminski AL, Burdick JA. Rational Design of Network Properties in Guest-Host Assembled and Shear-Thinning Hyaluronic Acid Hydrogels. Biomacromolecules. 2013; 14:4125–4134. [PubMed: 24070551]
25. Rodell CB, et al. Injectable Shear-Thinning Hydrogels for Minimally Invasive Delivery to Infarcted Myocardium to Limit Left Ventricular Remodeling. Circ. Cardiovasc. Interv. 2016; 9:e004058. [PubMed: 27729419]
26. Wang LL, et al. Injectable, Guest–Host Assembled Polyethylenimine Hydrogel for siRNA Delivery. Biomacromolecules. 2016; 18:77–86. [PubMed: 27997133]
27. Seif-Naraghi SB, et al. Safety and efficacy of an injectable extracellular matrix hydrogel for treating myocardial infarction. Sci. Transl. Med. 2013; 5:173ra25.
28. Guvendiren M, Lu HD, Burdick JA. Shear-thinning hydrogels for biomedical applications. Soft Matter. 2012; 8:260–272.
29. Mealy JE, Rodell CB, Burdick JA. Sustained small molecule delivery from injectable hyaluronic acid hydrogels through host-guest mediated retention. J. Mater. Chem. B. 2015; 3:8010–8019. [PubMed: 26693019]
30. Liu YM, et al. Cholesterol-conjugated let-7a mimics: antitumor efficacy on hepatocellular carcinoma in vitro and in a preclinical orthotopic xenograft model of systemic therapy. BMC Cancer. 2014; 14:889. [PubMed: 25429777]
31. Shim MS, Kwon YJ. Efficient and targeted delivery of siRNA in vivo. FEBS J. 2010; 277:4814–27. [PubMed: 21078116]
32. Wolfrum C, et al. Mechanisms and optimization of in vivo delivery of lipophilic siRNAs. Nat. Biotechnol. 2007; 25:1149–1157. [PubMed: 17873866]

33. Wang LL, Burdick JA. Engineered Hydrogels for Local and Sustained Delivery of RNA-Interference Therapies. Adv. Healthc. Mater. 2016; 6:1601041.
34. van de Manakker, Frank, van der Pot, Martin, Vermonden, Tina, van Nostrum, Cornelus F., Hennink, WE. Self-Assembling Hydrogels Based on β-Cyclodextrin/Cholesterol Inclusion Complexes. 2008; doi: 10.1021/MA702607R
35. López CA, et al. Molecular mechanism of cyclodextrin mediated cholesterol extraction. PLoS Comput. Biol. 2011; 7:e1002020. [PubMed: 21455285]
36. Politzer IR, et al. Effect of β-cyclodextrin on the fluorescence, absorption and lasing of rhodamine 6G, rhodamine B and fluorescein disodium salt in aqueous solutions. Chem. Phys. Lett. 1989; 159:258–262.
37. Mondal A, Jana NR. Fluorescent detection of cholesterol using β-cyclodextrin functionalized graphene. Chem. Commun. 2012; 48:7316.
38. López CA, de Vries AH, Marrink SJ. Molecular mechanism of cyclodextrin mediated cholesterol extraction. PLoS Comput. Biol. 2011; 7:e1002020. [PubMed: 21455285]
39. Senyo SE, et al. Mammalian heart renewal by pre-existing cardiomyocytes. Nature. 2012; 493:433–436. [PubMed: 23222518]
40. Ali SR, et al. Existing cardiomyocytes generate cardiomyocytes at a low rate after birth in mice. Proc. Natl. Acad. Sci. U.S.A. 2014; 111:8850–5. [PubMed: 24876275]
41. Snippert HJ, et al. Intestinal crypt homeostasis results from neutral competition between symmetrically dividing Lgr5 stem cells. Cell. 2010; 143:134–44. [PubMed: 20887898]
42. Lescroart F, et al. Early lineage restriction in temporally distinct populations of Mesp1 progenitors during mammalian heart development. Nat. Cell Biol. 2014; 16:829–40. [PubMed: 25150979]
43. Rios AC, Fu NY, Lindeman GJ, Visvader JE. In situ identification of bipotent stem cells in the mammary gland. Nature. 2014; 506:322–7. [PubMed: 24463516]
44. Sohal DS, et al. Temporally regulated and tissue-specific gene manipulations in the adult and embryonic heart using a tamoxifen-inducible Cre protein. Circ. Res. 2001; 89:20–5. [PubMed: 11440973]
45. Frank DB, et al. Emergence of a Wave of Wnt Signaling that Regulates Lung Alveologenesis by Controlling Epithelial Self-Renewal and Differentiation. Cell Rep. 2016; 17:2312–2325. [PubMed: 27880906]
46. Farin HF, et al. Visualization of a short-range Wnt gradient in the intestinal stem-cell niche. Nature. 2016; 530:340–3. [PubMed: 26863187]
47. Farin HF, Van Es JH, Clevers H. Redundant sources of Wnt regulate intestinal stem cells and promote formation of Paneth cells. Gastroenterology. 2012; 143:1518–1529.e7. [PubMed: 22922422]
48. Burdick JA, Prestwich GD. Hyaluronic acid hydrogels for biomedical applications. Adv. Mater. 2011; 23:H41–56. [PubMed: 21394792]
49. Tian Y, Morrisey EE. Importance of Myocyte-Nonmyocyte Interactions in Cardiac Development and Disease. Circ. Res. 2012; 110:1023–1034. [PubMed: 22461366]
50. Yang Y, et al. MicroRNA-34a Plays a Key Role in Cardiac Repair and Regeneration Following Myocardial InfarctionNovelty and Significance. Circ. Res. 2015; 117:450–459. [PubMed: 26082557]
51. Lesizza P, et al. Single-Dose Intracardiac Injection of Pro-Regenerative MicroRNAs Improves Cardiac Function after Myocardial Infarction. Circ. Res. 2017; 120:1298–1304. [PubMed: 28077443]
52. Monaghan MG, et al. Exogenous miR-29B Delivery Through a Hyaluronan-Based Injectable System Yields Functional Maintenance of the Infarcted Myocardium. Tissue Eng. Part A. 2017; doi: 10.1089/ten.TEA.2016.0527
53. Pandey R, et al. MicroRNA-1825 induces proliferation of adult cardiomyocytes and promotes cardiac regeneration post ischemic injury. Am. J. Transl. Res. 2017; 9:3120–3137. [PubMed: 28670398]
54. Patel RS, et al. High resolution of microRNA signatures in human whole saliva. Arch. Oral Biol. 2011; 56:1506–1513. [PubMed: 21704302]

55. Shcherbakova DM, Verkhusha VV. Near-infrared fluorescent proteins for multicolor in vivo imaging. Nat. Methods. 2013; 10:751–754. [PubMed: 23770755]

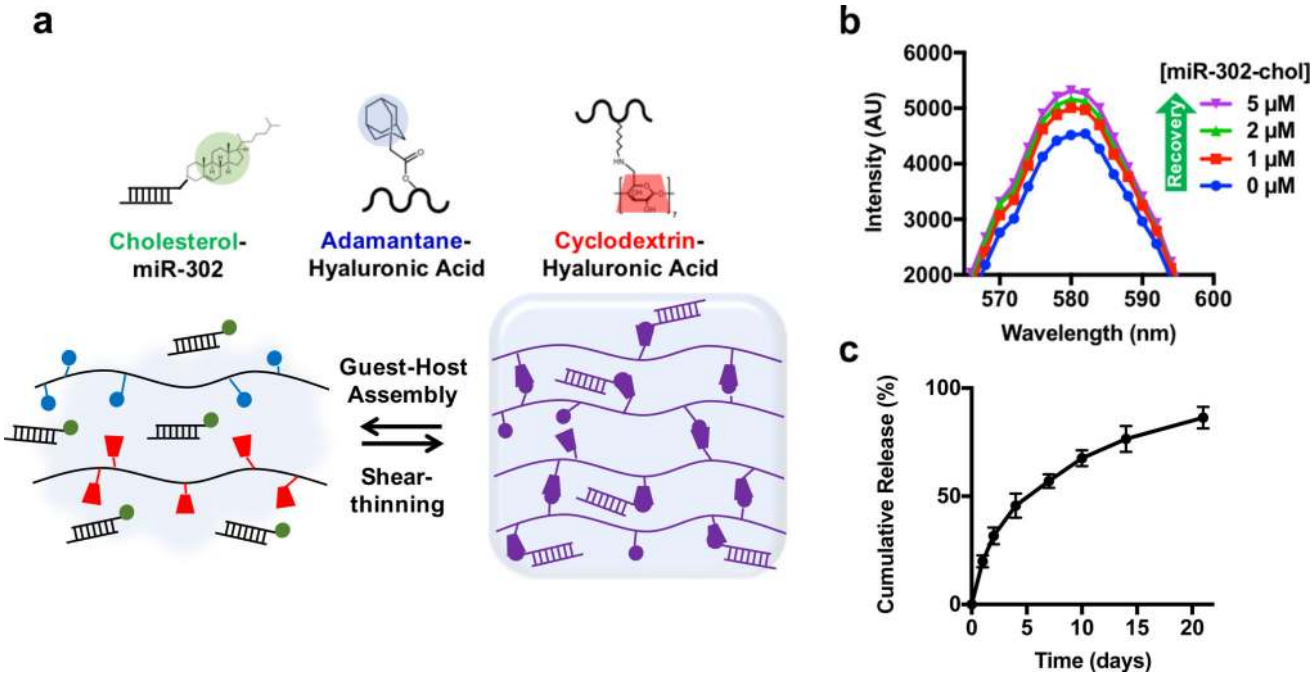

Figure 1. Gel assembly and miR-302 interactions

a) HA was modified with AD or CD, which self-assemble into shear-thinning and self-healing gels. Likewise, cholesterol on miR-302-chol interacts with CD to sustain release from the gel. b) Rhodamine/CD-HA interactions lead to quenching of rhodamine fluorescence, but the fluorescence is recovered by titration of cholesterol-modified miR-302 into the system and displacement of rhodamine complexes, indicating complexation between cholesterol and CD. c) Release of cholesterol-modified miR-302b and miR-302c (210 μM of each) from gels (5 wt%) in 1.5 mL microcentrifuge tubes over three weeks quantified by RiboGreen, a commercially available RNA quantification kit (mean ± SD, n=3).

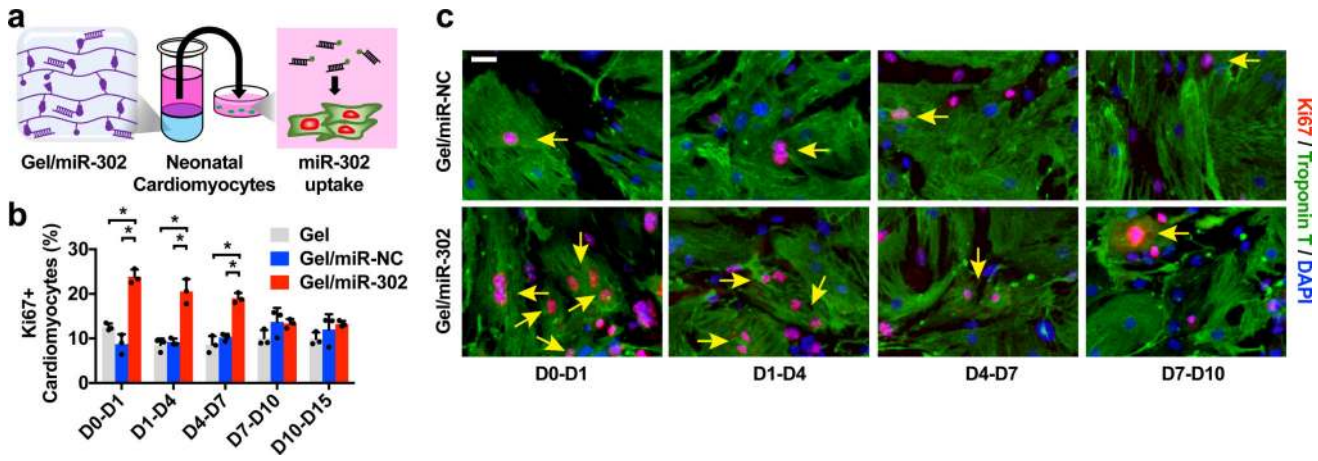

Figure 2. *In vitro* cardiomyocyte proliferation

a) Schematic of miR-302 supernatant collection and cardiomyocyte uptake. Gel/miR-302 (100 μL) assemblies were formed in 1.5 mL microcentrifuge tubes with cholesterol-modified miR-302 (210 μM of miR-302b and miR-302c) or miR-NC (420 μM). OPTI-MEM (500 μL) was added above gels and supernatant was collected, frozen, and replaced at D1, D4, D7, D10 and D15. Supernatants collected from each timepoint were added to primary neonatal cardiomyocytes in culture. At 48 hours, cardiomyocytes were stained for Ki67, cardiac Troponin T, and with DAPI to detect proliferation. b) Quantification of $Ki67^{+}cTnT^{+}$ neonatal cardiomyocytes from gel supernatants from D0-D1, D1-D4, D4-D7, D7-D10 and D10-D15 *in vitro* cultures demonstrating proliferative effects from early gel/miR-302 release out to 7 days (mean ± SD, n=3 per condition, *$p<0.05$). Quantification was based on counting of $Ki67^{+}cTnT^{+}$ co-stained cells relative to total $cTnT^{+}$ cells per high power field (HPF). c) Representative images of $Ki67^{+}cTnT^{+}$ neonatal cardiomyocytes (yellow arrows) to demonstrate increased Ki67 staining up to 7 days after exposure to gel/miR-302. Scale bar: 25 μm.

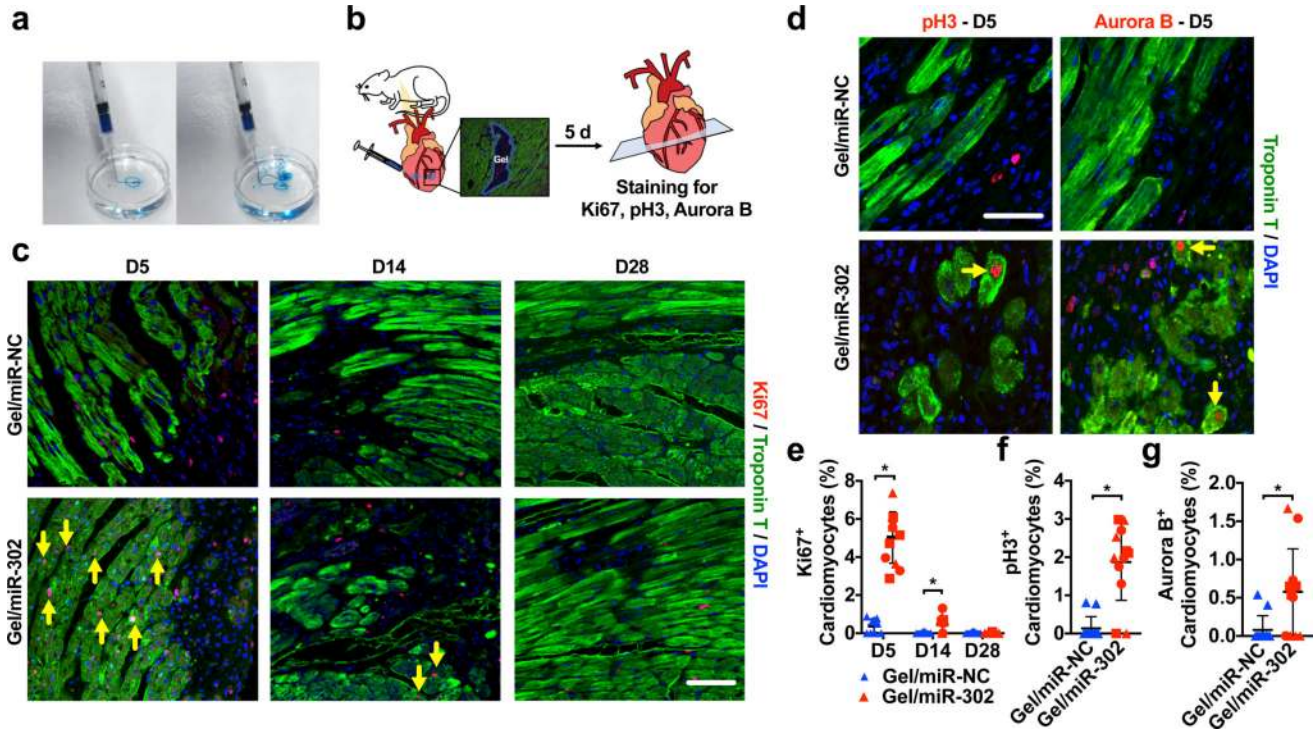

Figure 3. ***In vivo*** **cardiomyocyte proliferation**

a) Pre-formed gel (5 wt%, blue dye) injected from a 27Gx1/2" syringe into water, to demonstrate rapid reassembly and minimal dispersion of cargo upon injection. b) Schematic for intramyocardial gel injections into non-infarcted murine hearts. Two injections were made inferolateral to the proximal LAD below the left atrial appendage in non-infarcted mouse hearts after thoracotomy. At 5, 14, or 28 days, hearts were sectioned and stained for Troponin T and Ki67, pH3 or Aurora B. c) Representative images of Ki67 staining in cardiomyocytes (yellow arrows) and non-myocytes at D5, D14 or D28, demonstrating increased proliferation in gel/miR-302 treated hearts. Scale bar = 50 μm. d) Representative images of pH3 and Aurora B staining in cardiomyocytes (yellow arrows) at D5. Scale bar = 50 μm. e) Quantification of cardiomyocytes ($Ki67^+cTnT^+$) from hearts treated with gel/miR-NC or gel/miR-302, demonstrating sustained proliferation of cardiomyocytes f,g) Quantification of pH3 and Aurora B positive cardiomyocytes surrounding gel/miR-302 injection sites demonstrating increased proliferation in gel/miR-302 treated groups. Scale bar = 50 μm (mean ± SD, n=3 animals per group, symbol shapes indicate each animal, *$p<0.05$).

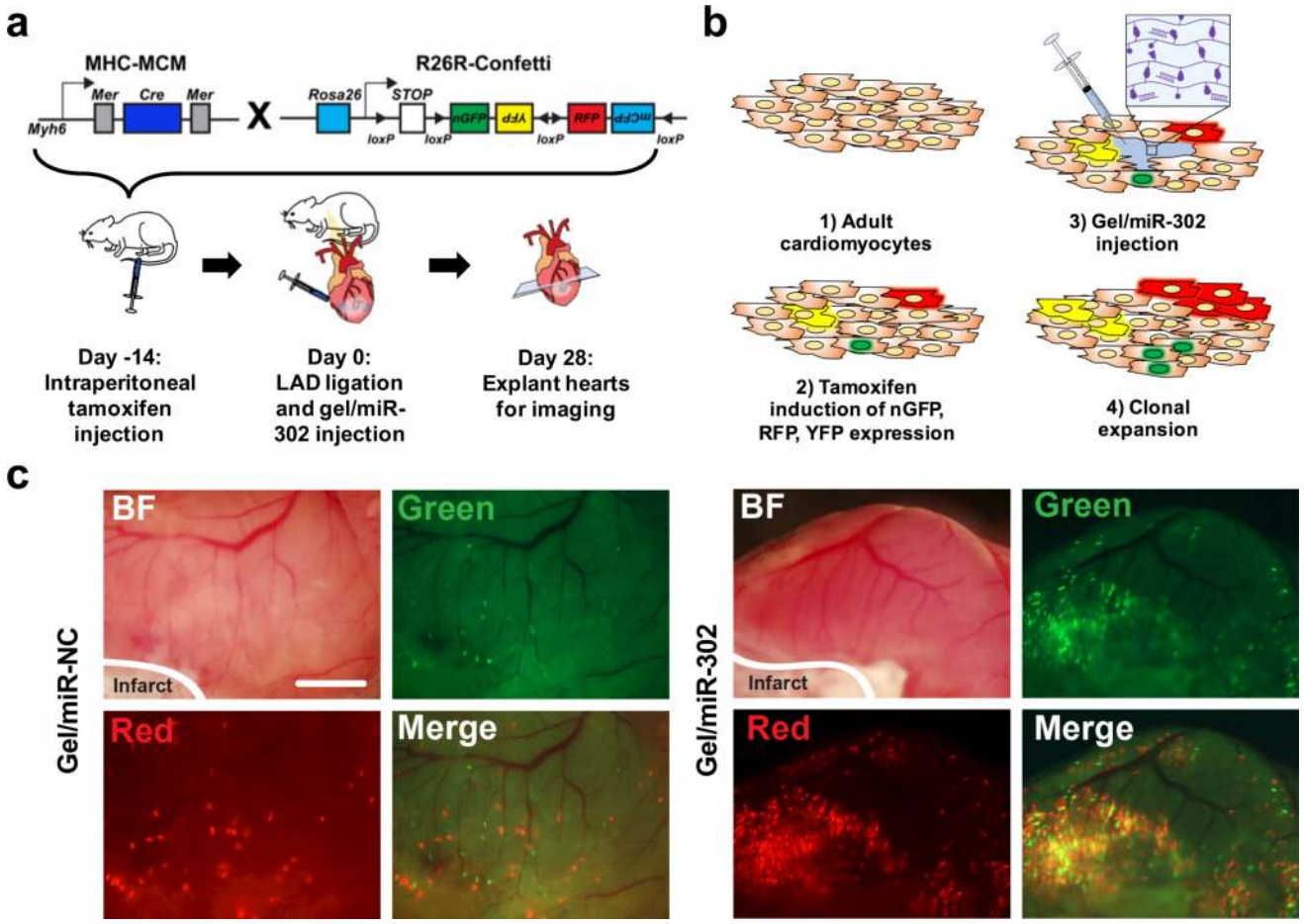

Figure 4. Gel/miR-302 induced clonal expansion *in vivo*

a) Schematic representation of lineage-tracing strategy and experimental design. To trace clonal proliferation, mice were cross-bred with Myh6^{MerCreMer} and R26R^{Confetti}. The expression of Myh6 leads to Cre-loxP recombination with consequent random activation of one of four fluorescent reporter proteins (nGFP, YFP, RFP and mCFP) with each color representing a different clone from a Myh6 positive cardiomyocyte. In our experimental design, mice were injected with tamoxifen intraperitoneally to induce the stochastic expression of nGFP, RFP, YFP and mCFP. After 14 days, the LAD was ligated to induce ischemic injury and gels were injected in the border zone of the infarct downstream. At 28 days after ligation, hearts were collected for analysis of clonal expansion. b) Mechanism for gel/miR-302 induced clonal expansion: 1) adult cardiomyocytes are non-proliferative and incapable of dividing after ischemic injury; 2) tamoxifen is used to randomly label a small population of cardiomyocytes with one of four fluorescent reporter proteins; 3) hearts are infarcted and gel/miR-302 is injected into cardiomyocytes in the border zone; and 4) miR-302 stimulates differentiation, proliferation, and expansion of fluorescently-labeled cardiomyocytes, which pass the fluorescent protein gene onto daughter cells. c) Fluorescent scans of gross heart specimens immediately after explanting at 28 days. Fluorescence is displayed in the green and red channels to indicate labeling of cardiomyocytes in both gel/miR-NC and gel/miR-302 treated groups. Scale bar = 2 mm.

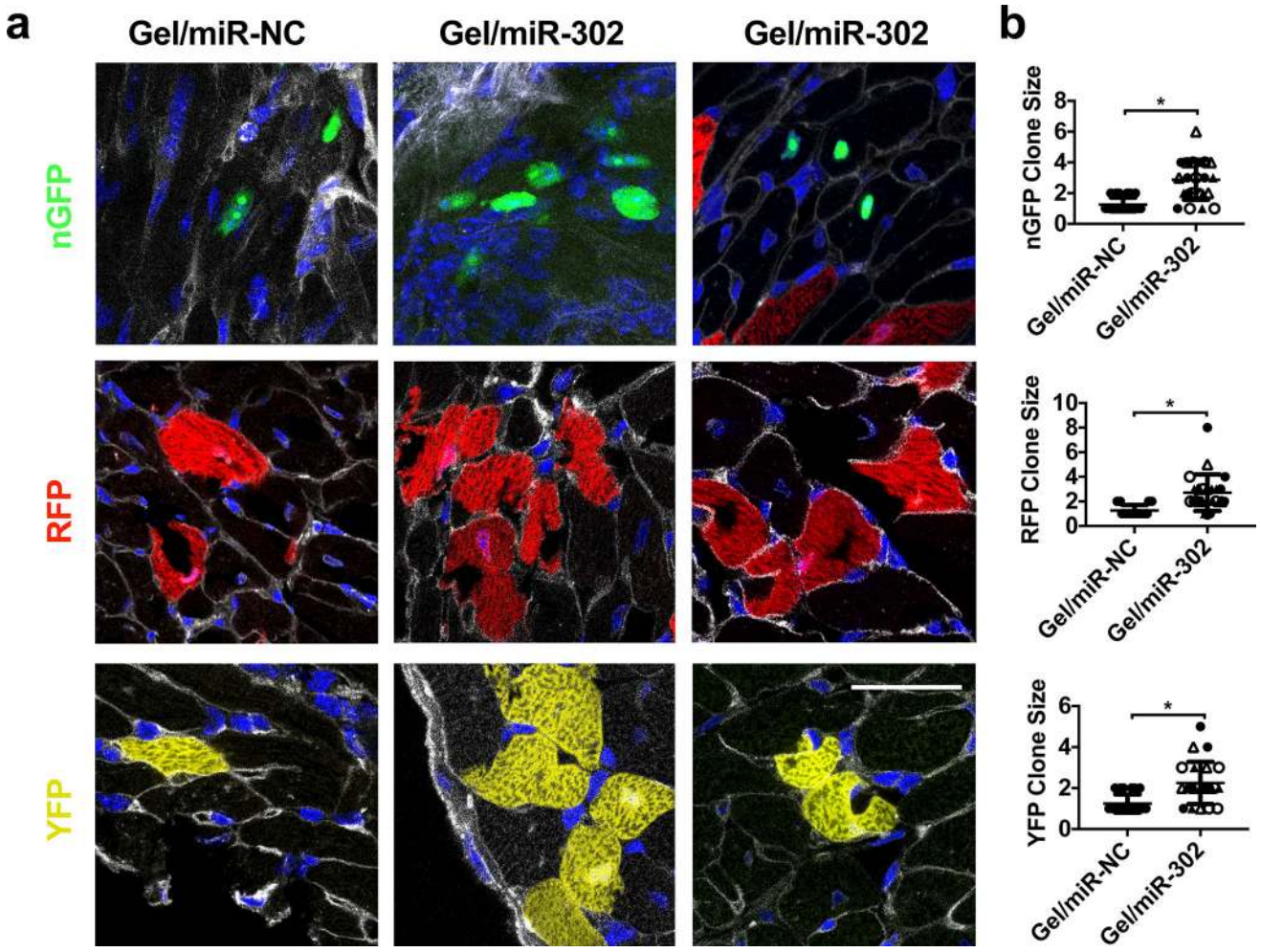

Figure 5. Clonal expansion of Confetti-labeled cardiomyocytes in mice

a) Representative sections from confocal imaging with labeled cardiomyocytes expressing nGFP, RFP, or YFP. Gel/miR-NC sections consisted mostly of individual cardiomyocytes that were spatially separated. In gel/miR-302 treated groups, multiple clones were observed in all three fluorescent channels in close proximity, consisting of several daughter cells from a single parent cell. WGA separates individual cardiomyocytes and permits identification of clones, specifically to differentiate multiple cardiomyocytes from multi-nucleated cardiomyocytes. Scale bar = 50 μm. b) Quantification of cells to a clone in the nGFP, RFP, and YFP channels. Clones are identified as cells within 50 μm proximity to one another (gel/miR-NC, n=3; gel/miR-302, n=4, symbol shapes indicate each animal, *$p<0.05$). Clones consisting of one cell are not technically clones but stochastically labeled single cells, but are still counted as part of the analysis to demonstrate they are the ubiquitous in the gel/miR-NC groups.

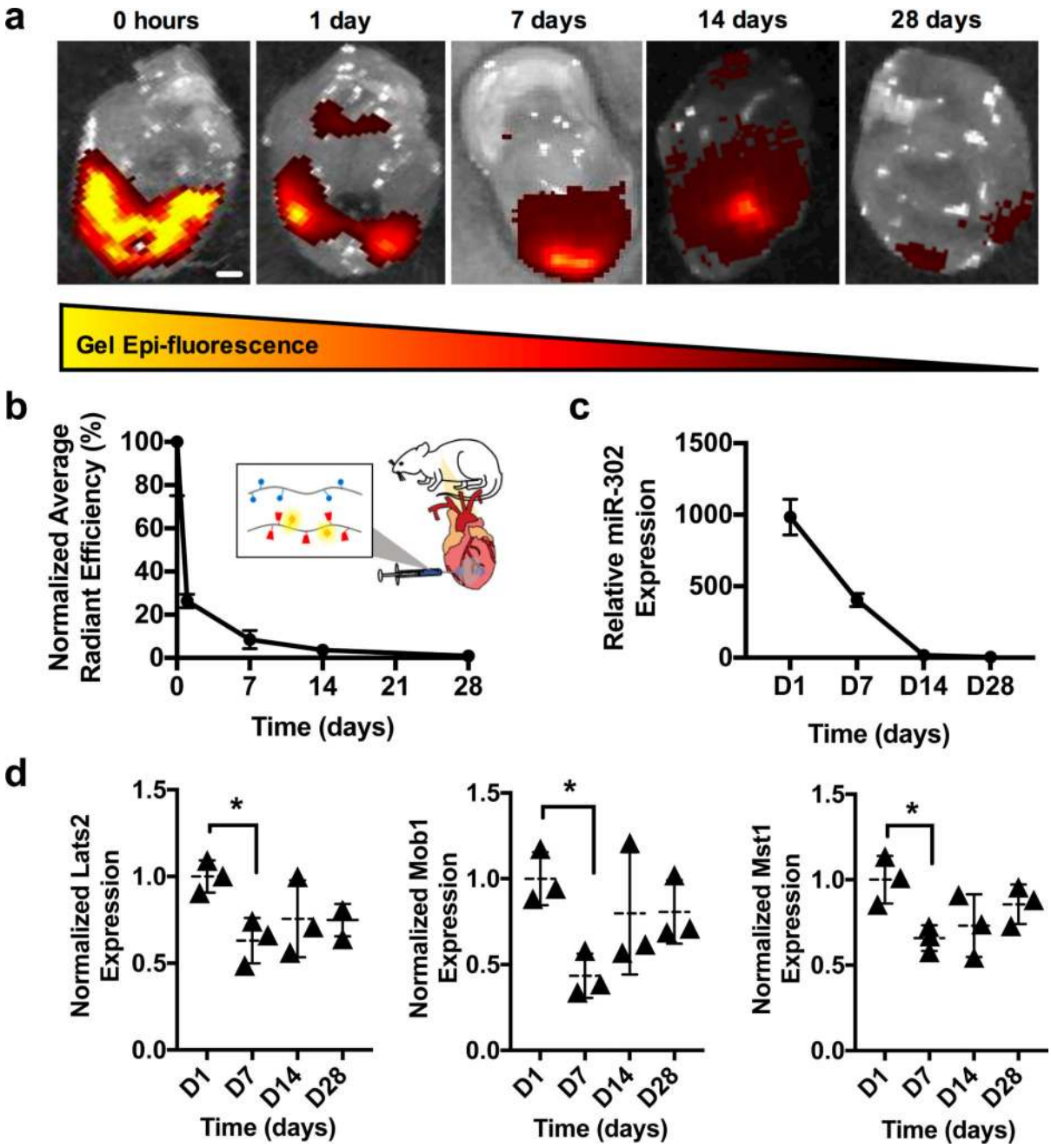

Figure 6. Gel and miR-302 retention in mouse hearts

a) Images of hearts explanted and scanned following Cy7.5-gel/miR-302 complex injection in MI model, demonstrating decreased gel epi-fluorescence over time. Scale bar = 1 mm. b) Quantification of total radiant efficiency by normalizing to the initial signal intensity and to background auto-fluorescence, demonstrating rapid clearance over the first week. c) qPCR quantification of miR-302 in the heart at various times following gel/miR-302 injection, normalized to miR-302 expression from gel/miR-NC, indicating sustained miR-302 expression (n=3 mice per timepoint). d) qPCR expression of miR-302 targets Lats2, Mob1,

Mst1 in gel/miR-302 treated mice normalized to gel/miR-NC treated mice (n=3 mice per timepoint, *p<0.05).

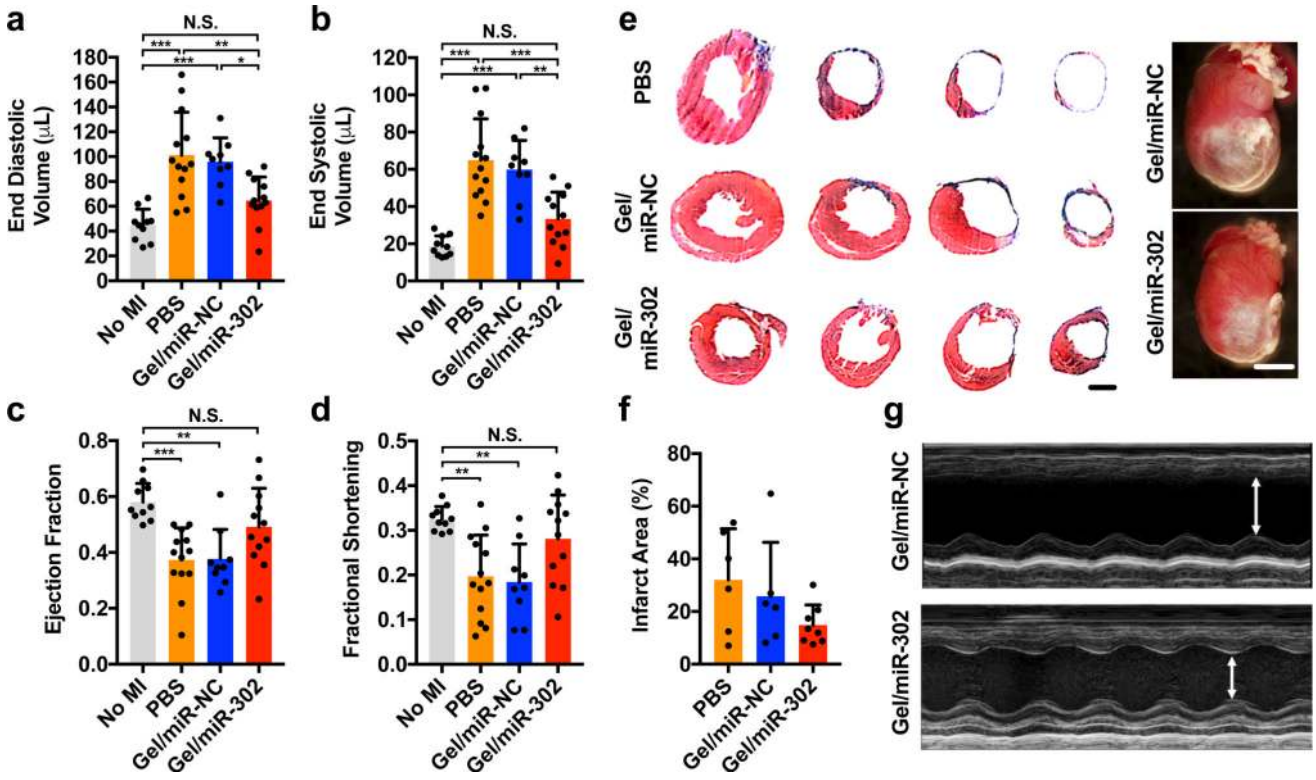

Figure 7. Functional outcomes after myocardial infarction in adult mice

a) End diastolic and b) end systolic volumes at 4 weeks after myocardial infarction in mice treated with PBS, gel/miR-NC, or gel/miR-302 by B-mode echocardiography. Volume increases were significantly decreased in gel/miR-302 treated groups compared to controls. c) Ejection fraction and d) fractional shortening at 4 weeks after myocardial infarction by echocardiography. Neither ejection fraction nor fractional shortening of gel/miR-302 treated mice were significantly different from non-infarcted mice. All groups were compared through 1-way ANOVA (Mean ± SD, no MI, n=10; PBS, n=13; gel/miR-NC, n=9, gel/miR-302, n=12. *p<0.05 **p<0.01 ***p<0.001). Outliers were removed using the robust regression and outlier removal method (ROUT) in Prism. e) Representative Masson's trichrome sections demonstrating cardiac volume improvement at 28 days. Sections are arranged from ligation to the apex to visualize changes in tissue remodeling. Scale bar (sections)= 2 mm. Scale bar (gross) = 5 mm. Representative gross heart pictures at D28 are also shown. f) Quantification of infarct size from gross sections. Infarct size was calculated from a minimum of three sections per animal where the scar was well-represented and expressed as Infarct Area (%) = (Infarct Area)/(Total Section Area). g) M-mode echocardiographs of left ventricular anterior and posterior walls demonstrating diminished motion in anterior wall of gel/miR-NC treated mice with improvement in gel/miR-302 treated mice.